Journal of Applied Phycology
https://doi.org/10.1007/s10811-022-02734-x

Salinity-induced chemical, mechanical, and behavioral changes in marine microalgae

N. Novosel[1] · T. Mišić Radić[1] · M. Levak Zorinc[1] · J. Zemla[2] · M. Lekka[2] · I. Vrana[1] · B. Gašparović[1] · L. Horvat[1] · D. Kasum[1] · T. Legović[1,3,4] · P. Žutinić[5] · M. Gligora Udovič[5] · N. Ivošević DeNardis[1]

Received: 21 December 2021 / Revised and accepted: 17 March 2022

Abstract

This study examines how salinity reduction triggers the response of three marine microalgae at the molecular and unicellular levels in terms of chemical, mechanical, and behavioral changes. At the lowest salinity, all microalgal species exhibited an increase in membrane sterols and behaved stiffer. The glycocalyx-coated species *Dunaliella tertiolecta* was surrounded by a thick actin layer and showed the highest physiological activity, negatively affecting cell motility and indicating the formation of the palmella stage. The lipid content of membrane and the hydrophobicity of cell were largely preserved over a wide range of salinity, confirming the euryhaline nature of *Dunaliella*. The species with calcite-encrusted theca *Tetraselmis suecica* exhibited the highest hydrophobicity at the lowest salinity of all cells examined. At salinity of 19, the cells of *T. suecica* showed the lowest growth, flagellar detachment and the lowest cell speed, the highest physiological activity associated with a dense network of extracellular polymeric substances, and a decrease in membrane lipids, which could indicate development of cyst stage. The organosilicate encrusted species *Cylindrotheca closterium* appeared to be salinity tolerant. It behaved hydrophobically at lower salinity, whereas becoming hydrophilic at higher salinity, which might be related to a molecular change in the released biopolymers. This study highlighted the interplay between chemistry and mechanics that determines functional cell behavior and shows that cell surface properties and behavior could serve as stress markers for marine biota under climate change.

Keywords Extracellular polymeric substances · Hyposalinity · Lipids · Microalgae · Motility · Nanomechanics

Introduction

Microalgae differ in their ability to survive and thrive in saline environments under the influence of osmotic stress (Helm et al. 2004). Because salinity can affect metabolic processes and water balance above or below the cell's isosmotic point (Kefford et al. 2002), microalgae have evolved various intracellular and extracellular osmoregulatory mechanisms to control osmotic stress in the face of salinity changes in the external environment (Gustavs et al. 2010; Shetty et al. 2019). At the cellular level, a change in salinity causes a variety of non-specific biochemical changes in the synthesis of active compounds, such as lipids, carbohydrates, carotenoids, steroids, sterols, and other secondary metabolites, changes in membrane permeability with a disruption of ion homeostasis (Benavente-Valdés et al. 2016; El-Kassas and El-Sheekh 2016; Minhas et al. 2016).

How microalgae adapt to environmental changes in salinity has been extensively studied (Borowitzka 2018a, b; Foflonker et al. 2018). The adaptive response of microalgae could be manifested by altering membrane fluidity, reducing protein synthesis, accumulating compatible solutes to maintain cell osmolarity, regulating photosynthesis to balance energy production and consumption (Barati et al. 2019; Pavlinska et al. 2020), and releasing extracellular polymeric substances (Decho and Gutierrez 2017; Ivošević DeNardis et al. 2019; Mišić Radić et al. 2021).

✉ N. Ivošević DeNardis
ivosevic@irb.hr

1 Ruđer Bošković Institute, Zagreb, Croatia

2 Institute of Nuclear Physics Polish Academy of Sciences, Kraków, Poland

3 Libertas International University, Zagreb, Croatia

4 OIKON-Institute for Applied Ecology, Zagreb, Croatia

5 Department of Biology, Faculty of Science, University of Zagreb, Zagreb, Croatia

Published online: 07 April 2022

The present study investigates the response of marine microalgae to salinity fluctuation in terms of chemical, mechanical, and behavioral changes to improve our understanding of the mechanisms and pathways through which a salinity stressor modulates the adaptive responses of microalgae at the individual cell level. Three widely distributed marine algal species, a biflagellate green alga with glycocalyx surface coating *Dunaliella tertiolecta*, a tetraflagellate green alga with calcite-encrusted theca *Tetraselmis suecica*, and a gliding diatom with organosilicate cell wall *Cylindrotheca closterium*, were studied at selected salinity levels that simulated changes from the euhaline to the mesohaline range of the salinity spectrum in marine systems.

Materials and methods

Cell suspensions

Three species of marine algae were selected as model organisms: *Dunaliella tertiolecta* (Chlorophyceae, CCMP 1320, Culture Collection Bigelow Laboratory for Ocean Sciences, Bigelow, MN, USA), *Tetraselmis suecica* (Chlorophyceae, CCAP 66 / 22A, Collection and Protozoa, Scottish Marine Institute, Oban, UK), and *Cylindrotheca closterium* (Bacillariophyceae, CCMP 1554, Culture Collection Bigelow Laboratory for Ocean Sciences). Cells were grown in 0.22-µm filtered natural seawater (salinity of 38), diluted to a specific salinity with MilliQ water, and then enriched with f/2 growth medium (Guillard 1975). Cultures were maintained in a water bath under controlled conditions (constant shaking (20 rpm), 12 h:12 h light to dark cycle with an irradiance of 31 µmol photons m^{-2} s^{-1}). Algal species were grown at four selected salinities of 9, 19, 27, and 38 (control). The average cell abundance in triplicate samples was determined using a Fuchs-Rosenthal hemocytometer. Growth rate and doubling time were determined in the exponential growth phase of algal cells (Kim 2015). Cells were harvested at stationary phase (15 days) by centrifugation (2000 × *g*, 3 min), and the washed pellets were resuspended twice with seawater of the corresponding salinity. The last pellet was resuspended in 2 mL of filtered seawater and served as the stock cell suspension.

Confocal microscopy

Confocal measurements were performed with a Leica TCS SP8 Laser Scanning Confocal Microscope (Leica Microsystems GmbH, Germany) equipped with a white-light laser and using a 63 × (N.A. = 1.4) oil immersion objective. The excitation wavelengths and emission ranges were optimized using the spectral scan option. A commercial dye SiR-Actin (excitation maximum 650 nm, detection range 670–700 nm) was used to visualize actin filament structures of *D. tertiolecta* and *T. suecica*. Visualization of the actin filament structures of *C. closterium* was not possible, probably because of its organosilicate cell wall. Autofluorescence of the algal cells was detected at an excitation maximum of 650 nm and a detection range of 720–750 nm.

Sample preparation for confocal imaging

The slides for confocal microscopy were washed in glass beakers with ethanol followed by ultrapure water. A stream of nitrogen was used to dry the slides. To prepare the slides for cell immobilization, 50 µL of 0.2% (w/v) polyethyleneimine (PEI, Sigma-Aldrich, USA) was added to the center of the clean slide and allowed to stand for 30 min. The PEI droplet was then removed and the center of the slide was rinsed three times with ultrapure water. The isolated algal cells (as described in the "Cell suspensions" section) were fluorescently labeled using the Sir-Actin kit (50 nmol Sir-Actin, 1 µmol Verapamil) from Tebu-bio (Ile-de-France, France). A stock solution of 500 µM Sir-Actin was prepared in anhydrous dimethyl sulfoxide (99.8% DMSO). To an aliquot of 50 µL of the washed cells, 0.5 µL of the Sir-Actin fluorescent dye was added. Finally, 20 µL of the stained cultures was added to the center of the glass slide and allowed to settle for 30 min. To prevent evaporation of the droplet, the slides were kept in a Petri dish with moist absorbent paper until imaging.

Motility analysis

Cell movements were recorded as 10 consecutive video files (.avi format, duration 5 s, 50–60 frames per second, image size: 340 × 250, 4 × 4 binning) under an Olympus BX51 microscope (10 × magnification). The video files were used as input to the open-source image processing software ICY (http:icy.bioimageanalysis.org) to analyze motility and trajectories of 1118 cells. Details of motility analysis are given in Novosel et al. (2020, 2021). The software package R (R Core Team, 2020) was used for additional statistical analyses. Box plots and plots of probability density distributions of speed and search radius were obtained. The distributions for different salinities were tested using the Shapiro normality test and the Wilcoxon-Mann–Whitney test.

Electrochemical method

The electrochemical method of polarography and chronoamperometry of oxygen reduction at the dropping mercury electrode (DME) was utilized to characterize the organic constituents, such as biopolymers and fluid microparticles in the aqueous electrolyte solution based on molecular adsorption or particle adhesion to the DME (Žutić et al.

1999, 2004; Svetličić et al. 2006; Pletikapić and Ivošević DeNardis 2017). Briefly, adsorption of organic molecules at the DME interface can be characterized by recording the polarographic maximum of Hg(II) ions, which is an alternative approach to measuring dissolved organic carbon in seawater (Hunter and Liss 1981). The surfactant activity of seawater is expressed as the equivalent amount of the nonionic synthetic surfactant Triton-X-100 (polyethylene glycol tert-octylphenyl ether) in milligram per liter. In contrast, the adhesion of fluid organic particles to the DME interface can be characterized by recording spike-shaped amperometric signals (Kovač et al. 2000; Svetličić et al. 2000; Ivošević DeNardis et al. 2007, 2012, 2015; Novosel et al. 2021). Whether the adhesion is spontaneous depends on the properties of the three interfaces in contact, based on the modified Young-Dupré equation (Israelachvili 1992).

Electrochemical measurements of algal cells

Electrochemical measurements of algal cell samples were performed in an air-permeable and thermostatic Metrohm vessel with a three-electrode system. The working electrode, the dropping mercury electrode, had the following characteristics: dropping time: 2.0 s, flow rate: 6.0 mg s^{-1}, maximum surface area: 4.57 mm^2. All potentials were referenced to a potential measured at a reference electrode, i.e., Ag/AgCl (0.1 M NaCl) separated from the measured dispersion by a ceramic frit. A platinum wire was used as the counter electrode. An aliquot of the cell suspensions was added to 25 mL of filtered seawater (pH 8.0) of the corresponding salinity and then poured into a Methrom vessel at 20 °C. Electrochemical measurements were performed using a 174A Polarographic Analyser (Princeton Applied Research, USA) connected to a computer. Analog data acquisition was performed using a DAQ card-AI-16-XE-50 (National Instruments, USA). Data analysis was performed using the application developed in LabView 6.1 software (National Instruments). Electrochemical characterization of the algal cell samples was performed by recording polarograms of oxygen reduction (current–potential curves) and current–time curves over 50 mercury drops at constant potentials (time resolution: 50 s). Signal frequency was expressed as the number of amperometric signals from the cells over a 100-s period. Surfactant activity was measured by adding 0.5 mL of 0.1 M $HgCl_2$ to the sample before measurement.

Atomic force microscopy imaging

Atomic force microscopy (AFM) imaging was performed using a Multimode Scanning Probe Microscope with Nanoscope IIIa controller (Bruker, USA) equipped with a 125 µm vertical engagement (JV) scanner. Contact mode imaging in air was performed with silicon nitride cantilevers (DNP, Bruker, nominal frequency of 18 kHz, nominal spring constant of 0.06 N m^{-1}). The linear scanning rate was between 1.5 and 2 Hz and the scan resolution was 512 samples per line. To minimize the interaction forces between the tip and the surface, the set point was kept at the lowest possible value. NanoscopeTM software (Bruker) was used to process and analyze the images.

Sample preparation for AFM imaging of cells and released extracellular polymers

Cells of *D. tertiolecta*, *T. suecica*, and *C. closterium* grown at salinities of 9, 19, 27, and 38, respectively, were separated from the growth medium by centrifugation as described in the "Cell suspensions" section. Unmodified mica was used as substrate for AFM imaging of *D. tertiolecta* and *C. closterium*, whereas polyethyleneimine (PEI; Sigma-Aldrich) modified mica was used for imaging of *T. suecica* (Novosel et al. 2021). The sample preparation protocol for AFM imaging required fixation of the *D. tertiolecta* suspension. A 5 µL aliquot of the cell suspension was pipetted onto freshly cleaved or PEI-modified mica and placed in a closed Petri dish for 1 h to allow the cells to settle and adhere to the surface. For rinsing, the mica was immersed in a glass of ultrapure water for 30 s three times and then dried. The mica discs were then taped to a metal sample pack with double-sided tape and imaged with the AFM.

Atomic force microscopy working in force spectroscopy mode

Measurements of the physical properties of the algal cells were performed using the Nanowizard IV AFM system (Bruker-JPK, Germany) in force spectroscopy mode in combination with an Olympus IX72 inverted optical microscope (Olympus Corporation, Japan). MLCT-D silicon nitride cantilevers were used to indent the algal cells. They were characterized by a nominal spring constant of 0.03 N m^{-1} and a half-opening angle of 21°. The spring constants of the cantilevers were calibrated using the thermal noise method (Sader et al. 1995). Measurements were made in the central region of the cell body regardless of the type of algal cells. However, in the case of *D. tertiolecta* and *T. suecica* cells, a scan area of 3 µm × 3 µm was chosen, over which a grid of 6 × 6 points was placed. For the cells of *C. closterium*, the size of the scan area was 1 µm × 1 µm, over which a grid of 2 × 2 points was defined. Force curves were recorded at an approach and retract velocity of 8 µm s^{-1} with a maximum force of 4 nN and curve lengths of 4 µm (*C. closterium* and *T. suecica*) and 6 µm (*D. tertiolecta*). Measurements were made at 18 °C in seawater at salinities of 9, 19, 27, and 38.

The recorded data, i.e., the force curves, were analyzed using JPK Data Processing Software (Bruker-JPK, Germany).

Young's modulus determination

The apparent Young's modulus (E) was determined by applying the Hertz-Sneddon contact model (Sneddon 1965). Here, the four-sided pyramid probe was used. Therefore, the relationship between the loading force F and the indentation depth δ is:

$$F = \frac{E'}{1-\mu^2}\frac{tan\alpha}{\sqrt{2}}\delta^2 \quad (1)$$

where E' is the reduced Young's modulus considering the elastic modulus of algal cells (E_{cell}) and cantilever (E_{tip}) is given by:

$$\frac{1}{E'} = \frac{1-\mu_{tip}^2}{E_{tip}} + \frac{1-\mu_{cell}^2}{E_{cell}}. \quad (2)$$

α is the open-angle of the tip, μ is the Poisson's ratio (μ_{cell} and μ_{tip} are Poisson's ratios related to the compressibility of the algal cells and indenting cantilever). Since $E_{\text{cell}} << E_{\text{tip}}$, the following approximation is obtained:

$$E' = \frac{E_{cell}}{1-\mu_{cell}^2}, \quad (3)$$

In our analysis, μ_{cell} equals 0.5 because we assume that the algal cells are incompressible. The maximum indentation depth did not exceed 1 µm, and the AFM data fit the model over a whole indentation range. The calculated E values were presented as box plots, distinguishing the median and the first (Q1) and third (Q3) quartiles.

The adhesive and hydrophobic properties of the algae were extracted from the retracting part of the force curve. They were quantified using the maximum work of adhesion (W_{adh}), defined as the area enclosing the negative force values. Hydrophilic (bare, silicon) and hydrophobic (trichlorooctadecylsilane (OTS, Sigma-Aldrich)) cantilevers were used to characterize the adhesive and hydrophobic properties of cell probes with different chemical properties. The functionalization of the OTS tips was performed by chemical vapor deposition. Silanization of the cantilevers was performed in a desiccator for 2 h, and the probes were used immediately. Scanning area, grid density, velocity, and the number of examined cells are specified in the "Atomic force microscopy working in force spectroscopy mode" section. The degree of hydrophobicity of the algal cell was defined as the difference between maximum adhesion values obtained for the interaction of the algal cell with untreated and CH_3-functionalized AFM cantilevers. It was quantified with $\Delta W_{\text{adh}} = W_{\text{adh (no OTS)}} - W_{\text{adh (OTS)}}$ (Novosel et al. 2021).

Sample preparation for force spectroscopy measurements

The protocol for sample preparation was recently published in Novosel et al. (2021). Briefly, algal cells were immobilized on a glass coverslip coated with PEI. The PEI was deposited by drop-casting technique (1 h), rinsed with seawater and dried with a stream of nitrogen. In the case of *C. closterium*, a 200-µL cell suspension was placed on a substrate for 1 h. The sample was then rinsed 3 times with 200 µL of filtered seawater. For *D. tertiolecta* and *T. suecica* cells, the following procedure was used. A volume of 1.5 mL of *D. tertiolecta* and *T. suecica* suspensions was centrifuged at 265 × *g* for 3 min and at 940 × *g* for 5 min, respectively. After removing 1 mL of the medium, the obtained pellet of algal cells was vortexed. Then, 1 mL of seawater was added and the cells were centrifuged at the same speed and duration. The supernatant was removed and the cells were suspended in 400 µL of the filtered seawater. Then, 100 µL of the cell suspension was placed on a PEI-coated glass slide for 30 min. Finally, the samples were rinsed 3 times with 100 µL of the filtered seawater.

Lipid extraction

Lipid extraction was performed from 50 mL of algal cell monoculture at the stationary growth phase. The sample was filtered through a pre-fired (450 °C/5 h) 0.7 µm Whatman GF/F filter. Extraction was performed using a modified one-phase solvent mixture of dichloromethane-methanol–water (Bligh and Dyer 1959): 10 mL of one-phase solvent mixture dichloromethane/methanol/deionized water (1:2:0.8 v/v/v) and 5–8 µg of standard methyl stearate (to estimate recoveries in subsequent steps of sample analysis) were added to the cut filters. They were then ultrasonicated for 3 min, stored overnight in the refrigerator, filtered through a sinter funnel into a separatory funnel, washed again with 10 mL of the one-phase solvent mixture and then once with 10 mL of dichloromethane/0.73% NaCl solution (1:1 v/v) and finally with 10 mL of dichloromethane. Lipid extracts collected in dichloromethane were evaporated to dryness under nitrogen flow and dissolved in 34 to 54 µL dichloromethane before analysis. All solvents were purchased from Merck Corporation (USA).

Lipid analysis

Lipid classes were determined by thin-layer chromatography with flame ionization detection (TLC–FID; Iatroscan MK-VI, Iatron, Japan). Lipids were separated on Chromarods S5. Quantification was determined by external calibration of lipid classes. Analysis was performed using a hydrogen flow of 160 mL min^{-1} and an airflow of

2000 mL min^{-1}. We determined representative membrane lipid classes: three glycolipids (GL) (monogalactosyldiacylglycerols (MGDG), digalactosyldiacylglycerols (DGDG), and sulfoquinovosyldiacylglycerols (SQDG)), three phospholipids (PL) (phosphatidylglycerols (PG), phosphatidylethanolamines (PE), and phosphatidylcholines (PC)), and sterols (ST). The total membrane lipid concentration was the sum of individual membrane lipids. The standard deviation determined from duplicate runs was 0–15%. The detailed procedure is described in Gašparović et al. (2015, 2017).

Results

Cell growth dynamics

Figure S1 shows the growth curves of three selected algal monocultures (*D. tertiolecta*, *T. suecica*, *C. closterium*) studied at four selected salinities (9, 19, 27, and 38). The initial number of inoculated cells in the growth media was similar for all species studied, approximately 4.0×10^4 cells mL^{-1}. All selected microalgae persisted in the salinity range from 9 to 38. The calculated growth rates and doubling times of three algae in the exponential growth phase at the salinity studied are summarized in Table S1. All microalgae had the shortest doubling time and fastest growth at salinity of 9.

Confocal images of algal cells grown at the corresponding salinities are shown in Figures S2–S4. Microscopic observations of *D. tertiolecta* at salinity of 27 showed no changes in autofluorescence or actin composition compared to cells grown at salinity of 38 (Figure S2a and b). At salinity of 19, *D. tertiolecta* cells build up actin layer (Figure S2c), which is particularly pronounced at salinity of 9 (Figure S2d). In addition, as observed in the transmitted light channel, at salinity of 9, some cells lost their flagella and became rounder, and the actin layer appeared thicker than in the control. No changes in autofluorescence or actin composition were observed in *T. suecica* over the entire range of salinity examined (Figure S3a-d). However, as observed in the transmitted light images, *T. suecica* cells tend to lose their flagella as salinity decreases. This effect was most evident at salinities of 19 and 9, where almost all cells have lost their flagella and the detached flagella accumulate around the cells. The cells of *C. closterium* maintained both shape and autofluorescent properties throughout the salinity drop (Figure S4a-d). As observed in the transmitted light channel, droplets accumulated inside the cells with decreasing salinity, although no trend was noted.

Motility characterization

Qualitative insights into the movement of *D. tertiolecta* cells at selected salinities are shown in Figure S5. At salinity of 9, approximately 66% of the cells (109 cells) were stationary or oscillating around a center (Tables S2.1), while the remainder (55 cells) exhibited considerable trajectories. At salinity of 19, a total of 68 cells were counted in the sample, of which about 57% (39 cells) were stationary. At salinity of 27, approximately 63% (41 cells) were stationary, while 37% (24 cells) exhibited considerable movement and were quantified. In contrast, at salinity of 38, most cells (79%) were in motion, while the minority (21%) were stationary.

Box plots of cell speeds of *D. tertiolecta* are shown in Fig. 1a.

The median of the speed at salinity of 9 was 29 μm s^{-1}, while the medians at salinities of 19 and 27 were identical: 50 μm s^{-1}. At salinity of 38, the median speed was significantly higher: 75 μm s^{-1}. The Shapiro test for normality yielded $p = 2.7 \times 10^{-10}$, 1.5×10^{-9}, 3.4×10^{-5}, and 1.8×10^{-6}, confirming that the density distributions of speeds were very far from normal. The Wilcoxon rank sum test showed that the density distributions of speeds were significantly different for cells grown at salinities of 9 and 19, 27 and 38, but not for cells grown at 19 and 27.

Because the group of cells that were stationary or vibrating around the center exhibited significantly different motion than the group of cells that were moving, it was important to note the speeds of the moving cells. The average speeds at salinities of 9, 19, 27, and 38 were 74 μm s^{-1}, 103 μm s^{-1}, 77 μm s^{-1}, and 81 μm s^{-1}, respectively (Table S2.2a).

Boxplots of the search radius of *D. tertiolecta* cells are shown in Fig. 1b. The median search radius at salinity of 9

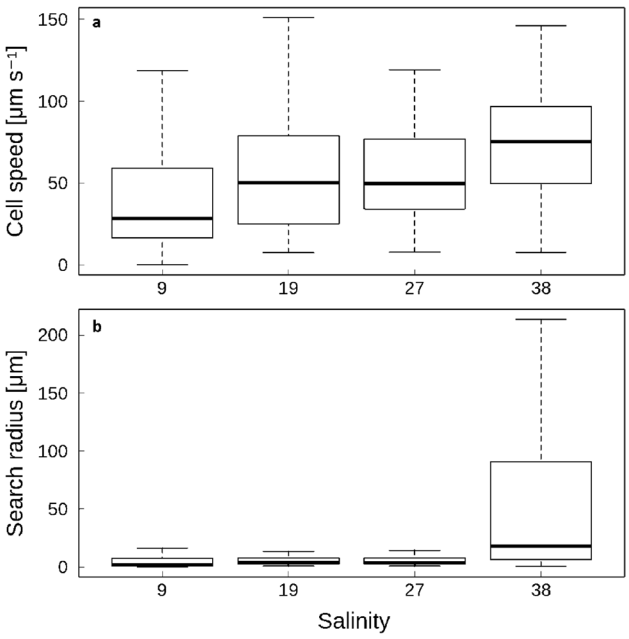

Fig. 1 Box plots of cell speed (**a**) and search radius (**b**) of *D. tertiolecta* grown at salinities of 9, 19, 27, and 38 (control)

was 2 µm, whereas the medians at salinities of 19 and 27 were 4 and 3 µm, respectively. At salinity of 38, the median search radius was significantly larger: 18 µm (Table S2.2.b). The Shapiro test for normality yielded $p = 2.2 \times 10^{-16}$, 7.3×10^{-16}, 2.1×10^{-13}, and 2.2×10^{-16}, respectively, confirming that all density distributions of the search radius were very far from normal. The Wilcoxon rank sum test showed that the density distributions of the search radius were significantly different for cells grown at salinities of 9 and 19, 27 and 38, but again not for cells grown at 19 and 27 ($p = 0.88$). The group of cells that moved consistently had an average search radius of 12 µm, 27 µm, 79 µm, and 72 µm at salinities of 9, 19, 27, and 38, respectively. In the same order of salinity, the linearity of motion was 0.1, 0.09, 0.32, and 0.45, respectively. Thus, the linearity was the same at salinities of 9 and 19 and 3 to 4.5 times smaller than at 27 and 38.

Qualitative insights into the movement of *T. suecica* cells grown at selected salinities are shown in Figure S6. At salinity of 9, approximately 43% of cells (35 cells) were stationary or showed oscillatory movement in place (Tables S3.1), whereas the majority of cells (46 cells) were clearly moving. At salinity of 19, a total of 124 cells were counted, with approximately 59% being stationary (73 cells). At salinity of 27, approximately 27% (26 cells) were stationary, while 73% (69 cells) showed significant movement and were quantified. In contrast, at salinity of 38, only 6% of cells were stationary, while 94% of cells moved vigorously.

Box plots of cell speeds of *T. suecica* are shown in Fig. 2a.

The median of the speed was 78 µm s^{-1} at salinity of 9, while the medians were 50 µm s^{-1} at salinity of 19 and 112 µm s^{-1} at salinities of 27. At salinity of 38, the median speed was significantly higher: 201 µm s^{-1} (Table S3.2a). The Shapiro test for normality yielded $p = 4 \times 10^{-4}$, 1.8×10^{-10}, 0.07, 8.8×10^{-5}, respectively. Only the density distribution at salinity of 27 did not deviate significantly from normality. The Wilcoxon rank sum test showed that the density distributions of speed were significantly different from each other, except for the distributions at salinities of 9 and 27, for which $p = 0.05$ was determined. The group of uniformly moving cells grown at salinities of 9, 19, 27, and 38 had an average speed of 124 µm s^{-1}, 155 µm s^{-1}, 137 µm s^{-1}, and 201 µm s^{-1}, respectively (Table S3.2).

Boxplots of the search radius of *T. suecica* cells are shown in Fig. 2b. The median search radius at salinity of 9 was 6 µm, while the medians at salinities of 19 and 27 were 4 and 12 µm, respectively. At salinity of 38, the median search radius was an order of magnitude larger: 102 µm (Table S3.2b). The Shapiro test for normality yielded $p = 4.6 \times 10^{-16}$, 2.2×10^{-16}, 6×10^{-16}, and 1.4×10^{-15}, respectively, confirming that all density distributions of the search radius are very far from normal. The Wilcoxon rank sum test showed that the density distributions of the search radii

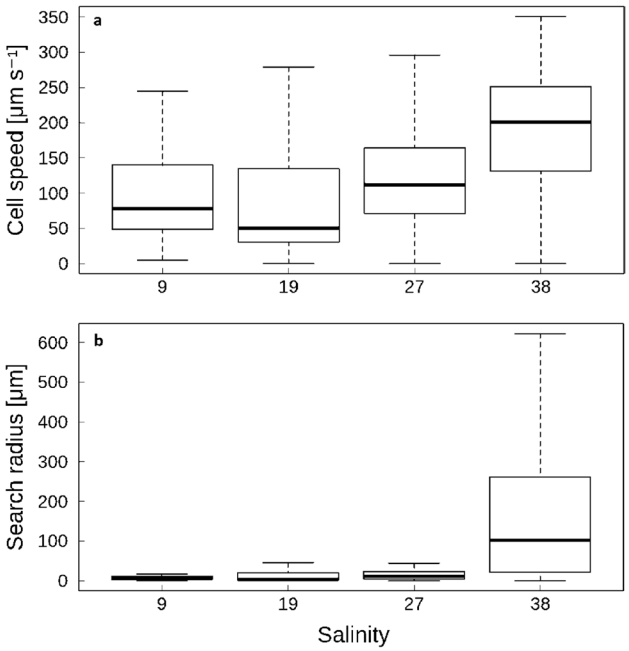

Fig. 2 Box plots of cell speed (**a**) and search radius (**b**) of *T. suecica* grown at salinities of 9, 19, 27, and 38 (control)

were significantly different from each other. The search radii of cells grown at salinities of 9 and 19 ($p = 0.027$) and cells grown at salinities of 9 and 27 ($p = 0.22$) were the narrowest. The group of significantly moving cells grown at salinities of 9, 19, 27, and 38 had an average search radius of 57 µm, 121 µm, 61 µm, and 174 µm, respectively. The linearity of moving cells with increasing salinity was 0.26, 0.58, 0.19, and 0.55, respectively, and reached the highest values at salinities of 19 and 38.

Electrochemical characterization of algal cells and released surface-active organic matter

The chronoamperometric curves for oxygen reduction recorded in the cell suspension of *D. tertiolecta* in seawater at potential of − 400 mV showed signals attributable to the adhesion of single cells to the charged interface (Fig. 3a).

The dependence of the signal frequency of *D. tertiolecta* grown at different salinities on the applied potentials is shown in Fig. 3b. The potential range of cell adhesion was defined with critical potentials of adhesion at the positively Ec^+ and negatively charged interface, Ec^-. The most negative and the most positive potentials, where at least one amperometric signal occurs per 10 consecutive *I-t* curves, correspond to the critical potentials (Žutić et al. 1993; Ivošević et al. 1994). The narrowest potential range of adhesion was recorded in the *D. tertiolecta* cell culture grown at salinity of 9, characterized by critical potentials of − 140 mV and − 990 mV in seawater, while the widest

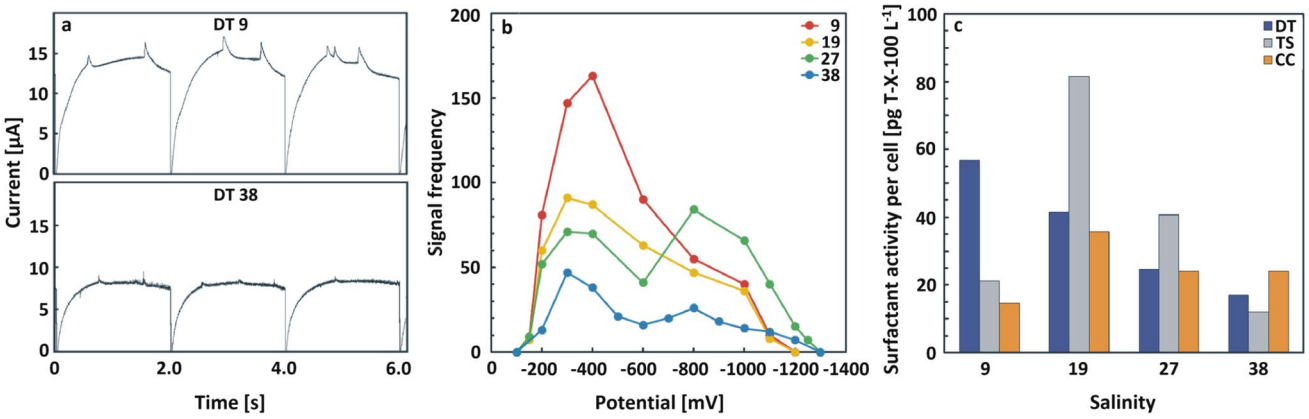

Fig. 3 Chronoamperometric curves for oxygen reduction at − 400 mV for three consecutive mercury drops recorded in *D. tertiolecta* cell suspension in seawater salinities of 9 and 38 (**a**); potential dependence of the signal frequency of *D. tertiolecta* cells grown at salinities of 9, 19, 27, and 38 (**b**); and surfactant activity for examined cell species at selected salinities (**c**)

potential range of cell adhesion was recorded in the cell suspension grown at 38 salinity, from − 110 to − 1240 mV, corresponding to favorable growth conditions. The frequency of amperometric signals increased with decreasing salinity due to the lower ionic strength of the medium, which was reflected in the increase in oxygen reduction current, thus enhancing the amperometric signals. The maximum number of amperometric signals occurred at potential of − 400 mV for all four salinities studied, as the interfacial tension is close to the maximum value (electrocapillary maximum). At potential of − 400 mV, the mercury electrode was positively charged and there was an electrostatic attraction between the positively charged interface and the negatively charged *D. tertiolecta* cells. By changing the potential in either direction, the interfacial tensions decreased and the number of amperometric signals from the cells decreased accordingly. At potential of − 800 mV, the mercury was negatively charged and the signal frequency decreased due to electrostatic repulsion with the negatively charged *D. tertiolecta* cells. Conversely, the chronoamperometric curves recorded in the suspensions of *T. suecica* and *C. closterium* were perfectly regular because there was no adhesion to the charged liquid interface due to cell rigidity (Novosel and Ivošević DeNardis 2021).

The electrochemical characterization of the released surface-active organic matter in the growth medium was determined by recording polarograms (current–potential curve) of Hg(II), which is proportional to the surfactant activity in the sample. The surfactant activity of the sample corresponded to a quantitative measure of the physiological activity of the cells in the growth medium. The data showed that the surfactant activity of the cells gradually decreased as follows: *T. suecica* (19) > *D. tertiolecta* (9) > *D. tertiolecta* (19) ~ *T. suecica* (27) (Fig. 3c).

Nanoscale imaging of algal cell and released extracellular biopolymers

Nanoscale imaging of single algal cells was performed at salinities of 9, 19, 27, and 38 (control). Regardless of salinity, all three species retained the same general cell shape. *Dunaliella tertiolecta* cells grown at all salinities tested had an ovoid shape with two flexible flagella. *Tetraselmis suecica* cells had an ellipsoidal shape at all salinities tested and the cell surface had granular structures corresponding to micropearls (Novosel et al. 2021). Most of the cells of *T. suecica* grown at salinity of 38 had flagella, and only half of the cells grown at salinity of 27 had flagella, whereas the cells grown at salinities of 9 and 19 had no flagella. The cells of *C. closterium* grown at all salinities tested had an elongated shape with flexible rostrae that could be clearly distinguished from the central part of the cell. Three morphologically distinct parts could be distinguished on the cell: the girdle band, the valve, and the raphe (Pletikapić et al. 2012; Novosel et al. 2021).

Based on AFM image analysis, the morphological parameters (length, width, height, and surface roughness) of cells grown at selected salinities are summarized in Table S4. The size of *D. tertiolecta* and *T. suecica* cells had the highest values at salinity of 38. The size of both, *D. tertiolecta* and *T. suecica*, grown at salinities of 9, 19, and 27 was similar and smaller than cells grown at 38. The roughness of *D. tertiolecta* cell surface was highest at salinity 38 and similar for salinities of 9, 19, and 27. The roughness of the cell surface of *T. suecica* was similar at all tested salinities. The length, width, and height range of *C. closterium* grown at salinities of 9, 19, and 27 were similar and greater compared with cells grown at salinity of 38.

The supramolecular organization of the released extracellular polymers (EPS) of *D. tertiolecta*, *T. suecica*, *and C. closterium* at selected salinities are shown in Fig. 4.

Around the cells of *D. tertiolecta* grown at salinities of 38 and 27, only globules and no fibrils or fibrillar networks were observed. Globules and some single fibrils were observed around the cells grown at salinity of 19. Around the cells grown at salinity of 9, a material consisting of globules, single fibrils and flat smooth structures was noted (Fig. 4a, b). The extracellular biopolymers around *T. suecica* grown at salinities of 9, 19, and 27 were in the form of a dense fibrillar networks and were located all around the cells, whereas no fibrillar material was observed at control salinity of 38 (Fig. 4c, d). The fibrils that formed the network ranged in height from 5 to 50 nm, with the highest network density found around the cells at salinity of 19 (Figure S7).

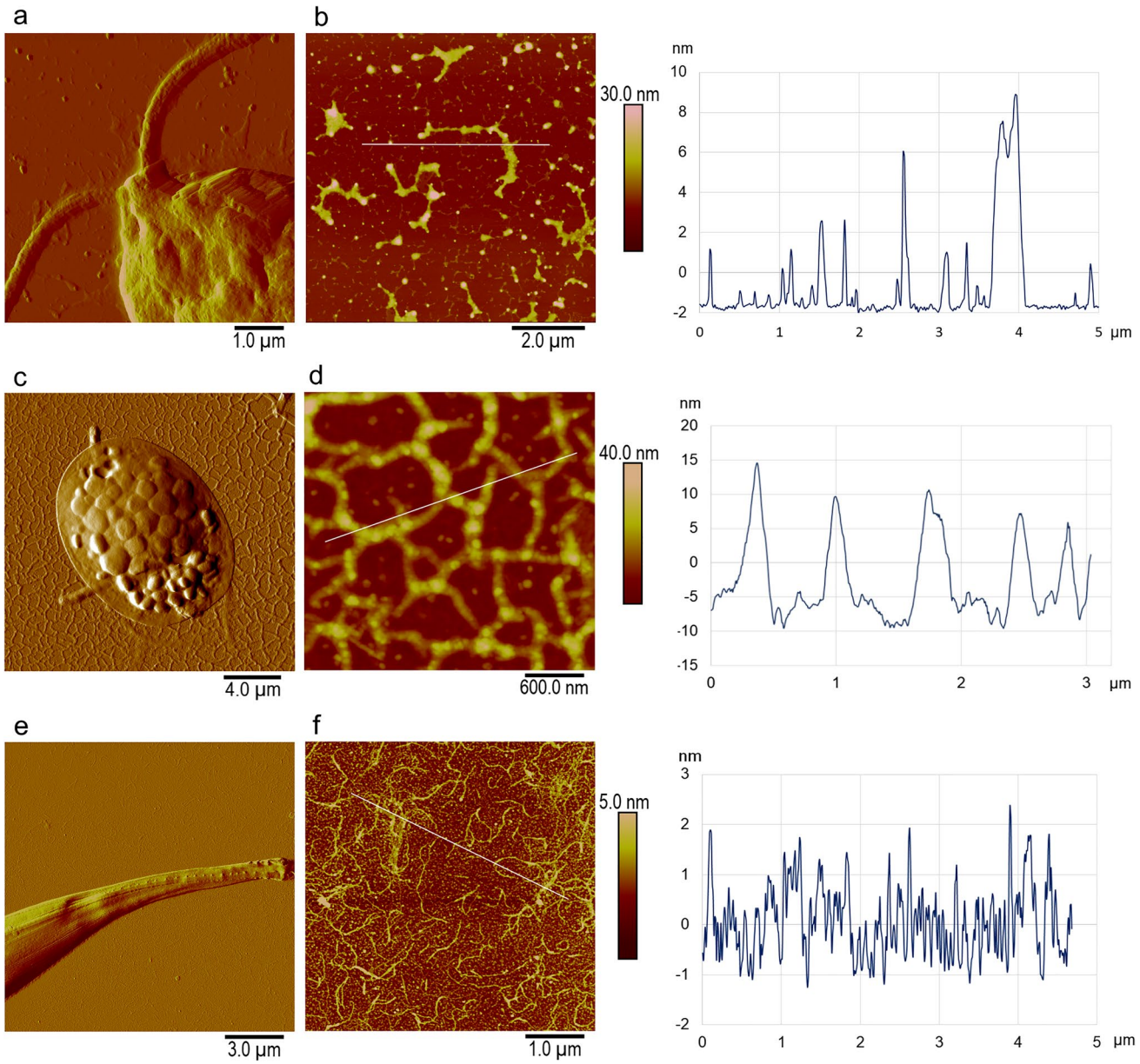

Fig. 4 AFM images of cells and extracellular polymers of *D. tertiolecta*, *T. suecica*, and *C. closterium* grown at selected salinities. Part of cell body with flagella of *D. tertiolecta* grown at salinity of 9 (**a**); EPS material around *D. tertiolecta* cell with vertical profile along indicated line (**b**); *T. suecica* cell grown at salinity of 19 (**c**); EPS network surrounding the *T. suecica* cell with vertical profile along indicated line (**d**); rostra of the *C. closterium* grown at salinity of 19 (**e**); EPS material around *C. closterium* with vertical profile along indicated line (**f**). Images are acquired using contact mode in air and presented as deflection (**a**, **c**, **e**) and height data with vertical profiles along indicated lines (**b**, **d**, **f**). Scan sizes: 6 µm×6 µm (**a**); 8 µm×8 µm, vertical scale 30 nm (**b**); 20 µm×20 µm (**c**); 3 µm×3 µm, vertical scale 40 nm (**d**); 15 µm×15 µm (**e**); 5 µm×5 µm, vertical scale 5 nm (**f**)

The extracellular biopolymers of *C. closterium* were in the form of single fibrils, locally cross-linked fibrils, and globules. For *C. closterium* grown at salinities of 9 and 19, a denser EPS material around the cells was noted and the fibrils exhibited a higher degree of cross-linking (Fig. 4e, f), whereas *C. closterium* grown at salinity of 27 had a lower degree of cross-linked fibrils near the cells, while single fibrils were mostly observed further from the cells.

Nanomechanical characterization of algal cells by AFM

The local elastic properties (E) of algal cells were quantified using the apparent Young's modulus calculated for the maximum indentation depth. At salinity of 38 (control), the cells of *D. tertiolecta* are characterized by the lowest E values. The cells of *T. suecica* are stiffer, while the local E values of *C. closterium* can be up to several MPa. The difference in mechanical response of these cells to compression could be due to differences in cell morphology. The cells of *T. suecica* are surrounded by close-fitting theca of fused organic scales. The cells of *C. closterium* contain stiff chloroplasts in the girdle band, and the cells of *D. tertiolecta* are covered only by the thick plasma membrane (Oliveira et al. 1980; Medlin and Kaczmarska 2004). Figure 5 shows the overlay of the box plots and Young's modulus distributions obtained for the algal cells of *D. tertiolecta*, *T. suecica*, and *C. closterium* cultured at salinities of 9, 19, 27, and 38, respectively.

Because the distributions of Young's moduli are broad and not symmetrical, we compared the median values of the cell populations studied. The median was accompanied by an interquartile range (IQR), which describes where the central 50% of the data lie (median (IQR). Statistical significance was determined using the Kruskal–Wallis ANOVA test ($p < 0.05$) to confirm differences between groups. Regardless of algal species, decreasing salinity increased the apparent Young's modulus (Fig. 5). The statistical significance for all groups was less than 0.0001 at the 0.05 level (Kruskal–Wallis ANOVA test) compared to the control group. Median (IQR) values obtained for *D. tertiolecta* cells increased from 3.5 kPa (3.2 kPa) at 38 to 8.6 kPa (7.6 kPa) at 27, 6.6 kPa (4.8 kPa) at 19, and 8.1 kPa (4.4 kPa) at 9, respectively. Statistical significance ($p < 0.05$) was also found for the measurements at salinities of 9 and 19, and at 19 and 27, whereas no statistically significant difference was found at salinities of 9 and 27. A similar trend of elastic modulus changes was observed in *T. suecica* cells. The cells were stiffer at low salinities, and $E(27) > E(9) > E(19)$. The corresponding medians were 138 kPa (190 kPa), 151 kPa (223 kPa), and 115 kPa (198 kPa), respectively. The value of E determined for *T. suecica* at salinity of 38 was 46 kPa (80 kPa). Weaker statistical significance was found between algal cells cultured at salinities of 9 and 27 ($p = 0.0011$), and

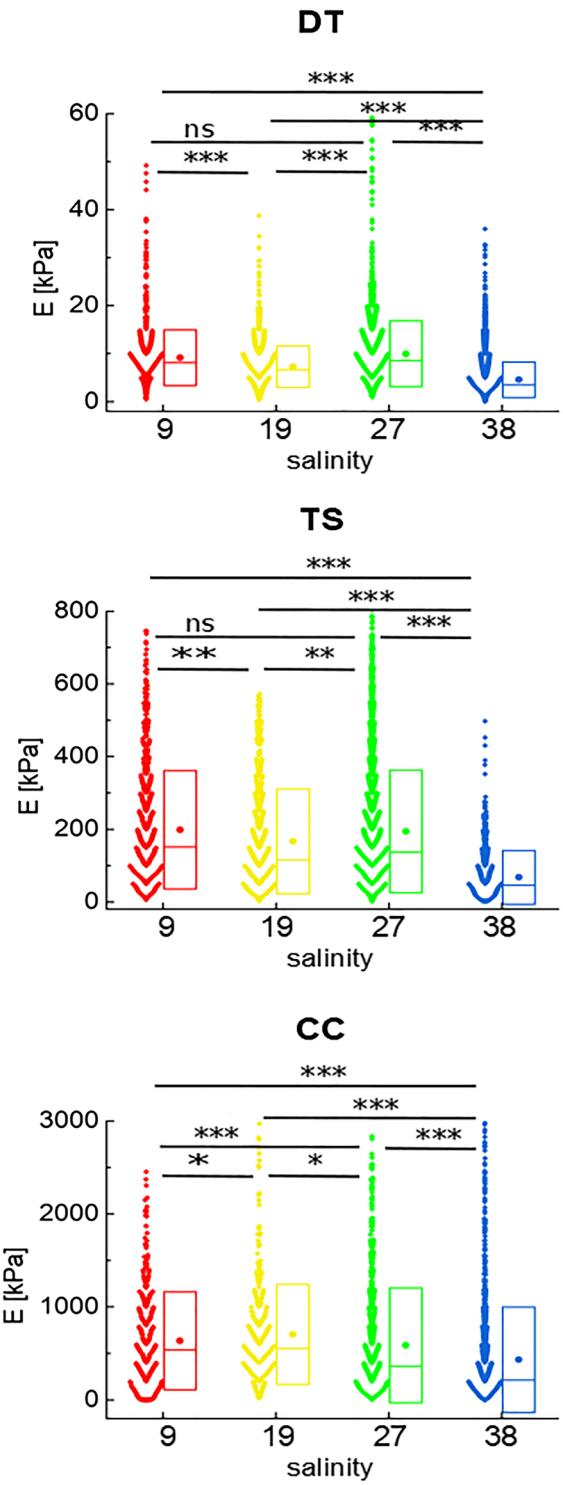

Fig. 5 Overlay of the box plots with Young's modulus distributions, obtained for *D. tertiolecta*, *T. suecica*, and *C. closterium* cells at salinities of 9, 19, 27, and 38. A box with whiskers represents a median ± interquartile range (Q3-Q1). Statistical significance was obtained from the Kruskal–Wallis ANOVA test at the level of 0.05 (*** $p < 0.001$, ns—not statistically significant)

19 and 27 ($p = 0.0019$). There was no statistical significance between cells of *T. suecica* cultured at salinities of 9 and 27. For *C. closterium*, the salinity stress increased the Young's modulus from 215 kPa (436 kPa) at normal conditions to 362 kPa (742 kPa) at salinity of 27. A further decrease in salinity to 19 and 9 was accompanied by an increase in the *E* to 553 kPa (532 kPa) and 537 kPa (759 kPa), respectively. The statistical significance for the 19 and 9 groups and 27 and 19 groups of *C. closterium* cells was less than 0.05, while the *p* value determined for the 9 and 27 groups was less than 0.001.

Adhesive and hydrophobic properties of algal cells

The adhesive properties, quantified by the maximum work of adhesion (W_{adh}), of algal cells grown at different salinities on chemically modified probes were studied. Cells were indented with hydrophilic (OTS −) and hydrophobic (OTS +) AFM probes. The change in hydrophobic properties (ΔW_{adh}) of the algal cell surface was determined by subtracting the work of adhesion determined for bare and OTS-coated cantilevers (Table S5): $\Delta W_{adh} = W_{adh(no\ OTS)} - W_{adh(OTS)}$. A positive value of ΔW_{adh} indicated that hydrophilic interactions dominate, while negative values indicated that hydrophobicity smothered the hydrophilicity. The mean values of the maximum work of adhesion (± standard error of the mean) obtained from measurements with bare and OTS-coated cantilevers are shown in Table S5.

We hypothesized that algal cells change their adhesion properties under salinity stress. Indeed, the hydrophobic properties of the cells changed depending on the salinity studied (Fig. 6), and these changes were species-dependent.

The resulting chemical properties of microalgae are shown in Figure S8. The data show that in the case of *D. tertiolecta*, the hydrophobic and hydrophilic properties were rather balanced, being characterized by low values of ΔW_{adh} (see Table S5). Only at salinities of 9 and 27 the cells became slightly more hydrophobic, as ΔW_{adh} is -0.018 ± 0.014 fJ and 0.047 ± 0.012 fJ, respectively. More pronounced salinity-dependent changes in surface properties were observed in *T. suecica* and *C. closterium*. At salinities of 38 and 27, ΔW_{adh} of *T. suecica* was close to zero. A further decrease in salinity resulted in high negative ΔW_{adh} values. In addition, we observed a significant decrease in the probability of adhesion to the bare AFM probe (P_{noOTS}), accompanied by an increase in P_{OTS} (see Figure S8 and Table S5). While the overall surface properties of *T. suecica* changed from balanced to hydrophobic with decreasing salinity, in the case of *C. closterium* we found that salinity can be a trigger between hydrophobic and hydrophilic surface properties. At salinity of 38, *C. closterium* cells had a hydrophilic surface ($\Delta W_{adh} = 0.0583 \pm 0.0072$ fJ). When the salinity decreased to 27, the ΔW_{adh} increased to 0.163 ± 0.085 fJ. Moreover, when

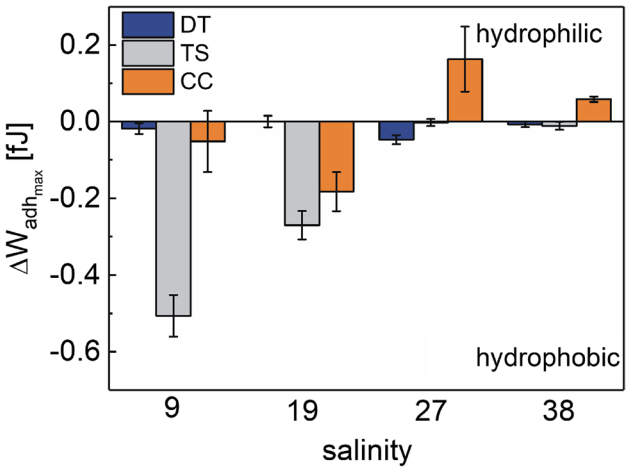

Fig. 6 The balance between hydrophilic and hydrophobic properties of algal cell surface plotted for salinities of 9, 19, 27, and 38. Data are presented as $\Delta W_{adh} \pm$ maximum error

the salinity decreased to 19, the relationship between the surface properties of the algal cells changed, and the cells of *C. closterium* became highly hydrophobic. At salinity of 9, the resulting work of adhesion was still negative. Moreover, the results of adhesion probability showed the affinity to hydrophilic materials depending on the structure and properties of the microalgal species (see Figure S8). *Dunaliella tertiolecta* showed a very low adhesion probability to the hydrophilic surfaces, in contrast to the cells of *C. closterium*, which preferentially adhered to the hydrophilic probe throughout the salinity studied. In the case of *T. suecica*, at salinities of 27 and 38, $P_{noOTS} > P_{OTS}$, while at salinities of 9 and 19, $P_{noOTS} << P_{OTS}$.

Lipid characterization of algal cells

The changes in cellular content of membrane lipids, ST, GL, and PL, caused by the decrease in salinity in the microalgal cell cultures of *D. tertiolecta*, *T. suecica*, and *C. closterium* are shown in Fig. 7.

In general, the least changes in total membrane lipids and classes with decreasing salinity were observed in *D. tertiolecta* (Fig. 7a, d, g, and j). In *T. suecica*, decreasing salinity resulted in a decrease in cellular content of total membrane lipids with a decrease of GL, followed by an increase of PL. In the microalga *C. closterium*, a decrease in total membrane lipid concentration, GL and PL was observed with a decrease in salinity from 38 to 9, but without a particular trend of change. Parallelly, a statistically significant ($p < 0.05$) increase in the cellular content of sterols was observed with the decrease in salinity in all three microalgae. At salinity of 9, the sterol content in diatom *C. closterium* was increased 3.8-fold compared to salinity of 38.

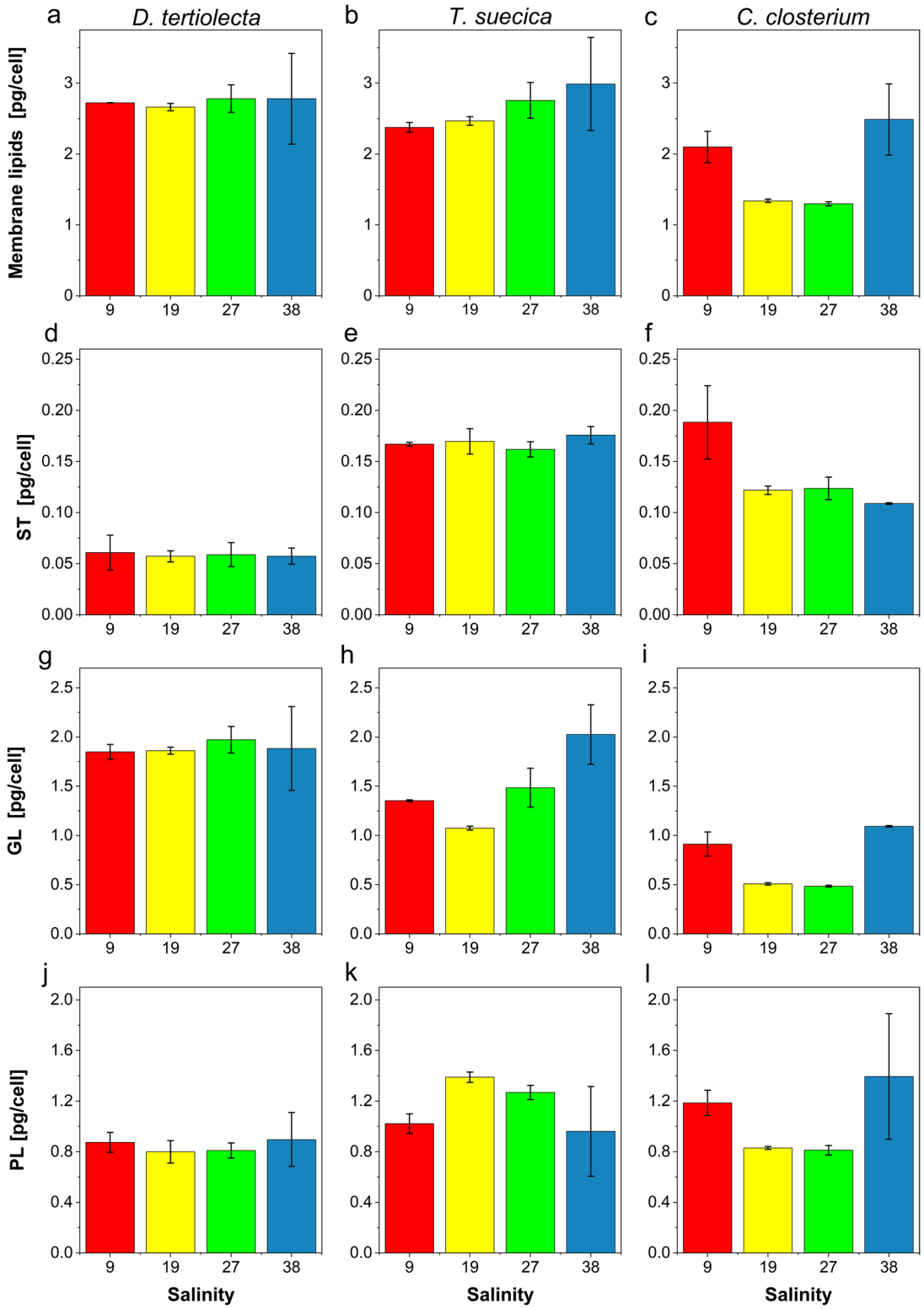

Fig. 7 Membrane lipid content of *D. tertiolecta* (**a**, **d**, **g**, and **j**), *T. suecica* (**b**, **e**, **h**, and **k**) and *C. closterium* (**c**, **f**, **i**, and **l**) at salinities of 9, 19, 27, and 38: total membrane lipids (**a**–**c**), sterols (ST) (**d**–**f**), glycolipids (GL) (**g**–**i**), and phospholipids (PL) (**j**–**l**). Data are shown as mean ± SD

However, the highest cellular sterol content was observed in *T. suecica* (Fig. 7e).

Discussion

We performed a comprehensive biophysical characterization at the level of a single algal cell to maintain structural integrity and clarify the poorly understood relationships between the chemical composition and mechanical properties of microalgae grown under selected salinity conditions. Three morphologically distinct marine microalgal species, *D. tertiolecta*, *T. suecica*, and *C. closterium*, were grown under four salinity conditions to mimic the broad salinity range in marine systems. We used a workflow that included chemical characterization (membrane lipids, hydrophobicity), nanomechanical characterization (stiffness), and behavioral characterization (physiological activity, motility, and adhesion to an interface) of microalgae in the stationary growth phase.

The responses of microalgae subjected to different salinity may also reflect cellular stress, resulting from the short-term salinity stress imposed on the cells which could trigger various morphological and biochemical changes (Borowitzka 2018b). Microalgae respond to abiotic stress through numerous mechanisms, including the adaptation of lipid composition and quantity to the new conditions. In response to various external stimuli, many microalgal species have evolved the ability to efficiently modify lipid metabolism by switching between nonpolar storage lipids (Thompson 1996; Guschina and Harwood 2006) and polar structural lipids. Storage lipids, composed mainly of polyunsaturated fatty acids are important for maintaining spontaneous curvature and flexural rigidity of membranes (De Carvalho and Caramujo 2018), while structural lipids are responsible for membrane fluidity, cell signaling pathways, and response to changes in the cellular environment (Aratboni et al. 2019; Rogowska and Szakiel 2020). Sterols are integral nonpolar components of eukaryotic membranes where, together with phospholipids, they regulate membrane permeability and fluidity and play an important role in sensing osmotic changes (Zelazny et al 1995). Notably, the cells of *T. suecica* were found to have the highest sterol production, in contrast to those of *D. tertiolecta*. In all three microalgae studied, total cellular concentrations of ST increased with decreasing salinity, indicating decreased membrane fluidity and increased cell hydrophobicity (Figs. 5 and 7). In contrast to the effects of decreasing salinity examined in our study, most studies of microalgal salinity accommodation examined the effects of higher than optimal salinity on lipid metabolism. Responses of *D. tertiolecta* and *Dunaliella salina* to growth in salinity concentrations above those of seawater resulted in a decrease in total sterol yield (Francavilla et al. 2010).

Profiling of microalgal membrane lipids is species- and abiotic stressor-specific (Ahmed et al. 2015; Novak et al. 2019). While changes in total PL and GL were observed in *T. suecica* and *C. closterium*, *D. tertiolecta* slightly altered cellular membrane lipid content. As observed in our concurrent study, the minimal but statistically significant changes in lipid remodeling in *D. tertiolecta* in response to low salinity (3) are attributed to the fact that *D. tertiolecta* is genetically adapted to large salinity fluctuations through polar lipid composition (Vrana et al. under revision). The fact that no linear response to salinity reduction was observed in *T. suecica* and *C. closterium* may indicate a change in nutrient and light availability for growth at different salinities. Similarly, no trend in total lipid content was observed in *T. suecica* growing in a salinity range of 15–90 g L^{-1} (Venckus et al. 2021).

As an euryhaline species, *D. tertiolecta* largely maintained membrane lipid content and hydrophobicity across the studied salinity range. When salinity decreased to 9, *Dunaliella* species became stiffer, which was accompanied by an increase in sterols, the formation of a thick actin layer, and pronounced physiological activity in the form of globular structures, which could indicate the transitioning of cells into palmella stage (Wei et al. 2017). Salinity-induced changes in cell stiffness would consequently affect cell adhesion behavior at the interface. The adhesion of *D. tertiolecta* cultured at salinity of 9 exhibited a narrow potential range, suggesting that the cells were stiffer and more hydrophobic than those cultured at salinity of 38 (Fig. 3b). These observations were consistent with the nanomechanical characterization of *Dunaliella* cells at selected salinities. Aging of *Dunaliella* cells also leads to changes affecting cell stiffness, hydrophobicity, and adhesion behavior, which may be related to molecular modification of the cell envelope (Pillet et al. 2019).

The second species, a calcite-encrusted thecate *T. suecica*, showed the most pronounced salinity-related changes which could indicate the formation of a cyst stage. At salinity of 9, cell exhibited the loss of flagella, the highest cell stiffness and hydrophobicity, accompanied by an increase in ST content and a decrease in GL content, which affected the distribution of surface charges and accordingly caused changes in the adhesive properties of the microalga (Figs. 6 and 7, Fig. S8). At salinity of 19, *T. suecica* showed the most pronounced physiological activity among all the species studied in the form of a dense EPS network (Figs. 3c and 4, Fig. S7), which was accompanied by a decrease in total membrane lipid content (Fig. 7b). A fundamental role in EPS production is played by variation in salinity, which exerts oxidative stress on cells and affects cellular ion balance (Guzman-Murillo and Ascencio 2001; Parra-Riofrío et al. 2020). At lower salinity, cellular ion concentrations increased and their ion ratios were constant, whereas at

salinity higher than 20, ion ratios became variable (Kirst 1990), affecting the amount of EPS production in *T. suecica* and its adaptation mechanisms to osmotic stress (Guzman-Murillo and Ascencio 2001).

Cylindrotheca closterium, a species enclosed within an organosilicate frustule, showed good adaptation to a wide range of salinity (Glaser and Karsten 2020). At lower salinities of 9 and 19, the cells of *C. closterium* showed hydrophobic behavior, whereas at higher salinities of 27 and 38, they showed a hydrophilic character accompanied with physiological activity (Figs. 3c and 6). This result could suggest that the observed salinity-induced transition of *C. closterium* cell properties from hydrophobic to hydrophilic might be related to the amount and ratio of sulfated (sPS) and carboxylated (cPS) polysaccharides, as has been reported for the adaptation of marine species to high salinity environments (Aquino et al. 2011; Arata et al. 2017). In this way, EPS composition mainly determined the adhesiveness of algal cells (Xiao and Zheng 2016). Whether a microalgal cell behaves hydrophobically or hydrophilically determines its ecological role in marine systems, whether they live in the benthos and/or form colonies or live as plankton (Griffiths and Harrison 2009; Ozkan and Berberoglu 2013; Novosel et al. 2021).

At the nanometer level, the morphology of microalgal cells did not show any specific changes, except for the change in cell size and the loss of flagella in the cells of *T. suecica*. The cells of *D. tertiolecta* and *T. suecica* grown at lower salinities were smaller than those grown at a salinity of 38. These results are consistent with the commonly known fact that phytoplankton cell size decreases not only with temperature (Atkinson et al. 2003) but also with decreasing salinity (Litchman et al. 2009). Fu et al. (2014) showed that the cell volume of *D. salina* fluctuated continuously for 10 days as a result of high salinity stress, eventually stabilizing at a slightly larger cell size compared to unstressed conditions. The loss of flagella in the cells of *T. suecica* grown at lower salinity could indicate development of cyst stage, as has been reported for other flagellated microalgae (Borowitzka and Siva 2007; Ma et al. 2012; Wei et al. 2017; Shetty et al. 2019; Hyung et al. 2021). On the other hand, the cells of *C. closterium* were larger compared to cells grown at salinity of 38, presumably not only related to salinity but also to its life cycle, in which the maximal cell size is attained by initial cells sprouting from the fully grown auxospores (Vanormelingen et al. 2013).

Reducing the salinity from 38 to 9 resulted in a much higher secretion of biopolymers in all species, which allowed the stressed cells to survive under unfavorable conditions. The extracellular biopolymers secreted by stressed *D. tertiolecta* cells changed their supramolecular structure with decreasing salinity, i.e., the spherical structure observed at salinity of 38 changed to a fibrillar structure at salinity of 9. Fibrillar structures were also present when cells were grown at a lower temperature (Novosel et al. 2021). The greatest difference in EPS organization was observed in *T. suecica* cells. Cells grown at salinities of 9, 19, and 27 released fibrillar networks, with the highest network density observed at salinity of 19 (Figure S7), which is similar to dense EPS network formation of *C. closterium* cells at 30 °C. In contrast, only spherical material was present around *T. suecica* cells exposed to temperature stress (Novosel et al. 2021).

At the population level, rapid and quantitative high-throughput analysis of several hundred cells allowed characterization of microalgal motility behavior (Novosel et al. 2020). Microalgal motility behavior depends on the complexity of the flagellar system. For example, biflagellated *Dunaliella* cells had about 3 times lower cell speed than tetraflagellated *T. suecica* (Figs. 1 and 2). Both cells showed that cell motility is dependent on salinity. At salinity of 9, the population of vibrating cells predominated, moving around the spot with minimal cell speed. When the salinity was increased to 38, the number of motile cells increased, and the cell speed and search radius increased accordingly. At salinity of 38, the search radius of both flagellar cells ranged from 6 to 13 body lengths per second and showed brisk movement. As cell motility can be influenced by cell physiological activity (Mayali et al. 2008), the pronounced cell physiological activity detected in *T. suecica* cell cultures at salinity of 19 could interfere with cell speed and search radius (Figs. 2, 3c, and 4c).

To place this study in a broader context, we compared the influence of individual abiotic stressors: temperature *vs.* salinity as the main environmental indicators of climate change on the adaptation response of selected microalgae in the stationary growth phase. A color wheel illustrating chemical, mechanical, and behavioral changes in terms of hydrophobicity, stiffness, EPS production, and motility of microalgae when exposed to a temperature maximum (Novosel et al. 2021) and salinity minimum is shown in Fig. 8.

Our results showed that the adaptive response of microalgae is species-specific and stressor-specific. Decrease in salinity triggered profound chemical, mechanical, and behavioral response in the studied microalgal cells. All three selected species became stiffer and behaved hydrophobically, while differing in physiological activity. Although cells of *T. suecica* are enclosed in a calcite-coated theca, they appeared to be sensitive to hyposaline conditions, as indicated by the highest hydrophobicity and physiological activity. In contrast, temperature did not elicit a major adaptive response in *T. suecica*, demonstrating a temperature tolerance. The green alga *Dunaliella*, which is surrounded by a glycocalyx layer, showed a profound chemical and mechanical response under both stressors, consistent with the extremophilic nature of *Dunaliella*. In contrast, the pennate diatom *C. closterium*,

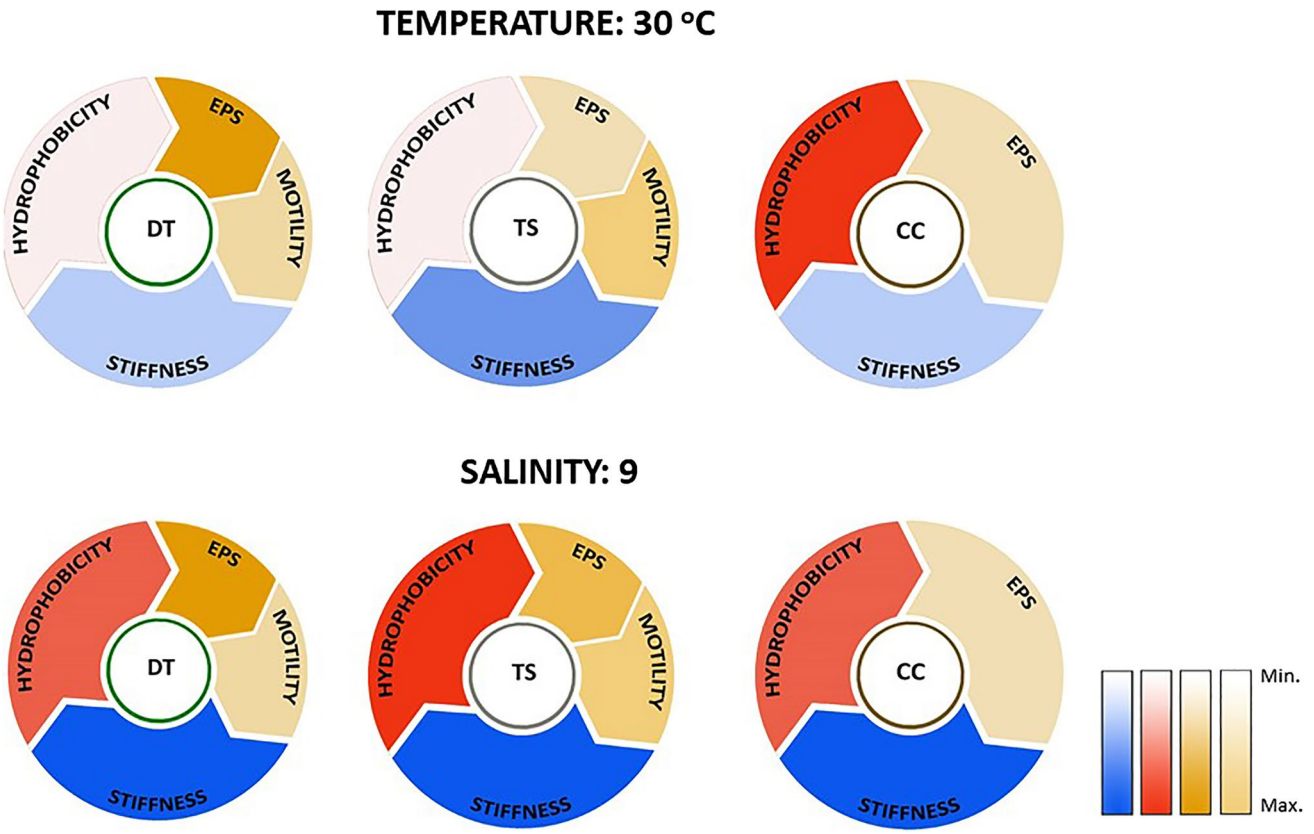

Fig. 8 Comparison of adaptive responses of microalgae triggered by individual stressors (temperature of 30 °C *vs*. salinity of 9). Temperature-induced adaptive responses of microalgae have been described in detail (Novosel et al. 2021). Color shading refers to the response of microalgae compared to control conditions (temperature of 18 °C and salinity of 38)

enclosed in an organosilicate frustule, maintained a nearly constant hydrophobicity and EPS production, regardless of the stressors studied. Such environmental adaptation of diatom cells derives from a long-lasting evolutionary advance in genetic, physiological, and morphological traits (Falkowski et al. 2004; Armbrust 2009).

Our results, based on a study conducted in the laboratory, showed that the adaptive response of algae to changes in abiotic stressors could be identified and quantified. In this way, the present fundamental study may help to understand how salinity controls the diversity, structure, and function of microbial communities in aquatic systems, with only those microorganisms that have successfully adapted to salinity being able to survive the ongoing and projected salinity fluctuations (Baek et al. 2011; Triadó-Margarit and Casamayor 2012; Bautista-Chamizo et al. 2018).

Conclusion

We investigated the salinity-induced adaptive response of two green microalgae and a diatom in the terms of chemical, mechanical, and behavioral changes. Our results showed that the adaptive response of microalgae is species- and salinity-specific. Although covered only with glycocalyx coat, the cells of *D. tertiolecta* adapt to a wide range of salinity levels without significant changes in membrane lipids and hydrophobicity, confirming their euryhaline nature. *Dunaliella tertiolecta* responded to a decrease in salinity to 9 with the formation of a thick actin layer, increase in cell stiffness, sterol content and physiological activity, and a decrease in motility, likely leading to the formation of a palmella stage. The cells of *T. suecica* proved to be sensitive to salinity fluctuations, despite being surrounded by a calcite-encrusted theca. In particular, a decrease in salinity to 19 in *T. suecica* resulted in growth reduction, loss of flagella, decrease in motility, increase in cell stiffness, hydrophobicity, sterol content, and the formation of a dense EPS network with a concomitant decrease in membrane lipids, which might indicate the progressing of cells into the cyst stage. *Cylindrotheca closterium*, enclosed in organosilicate frustule, proved to be tolerant to a decrease in salinity. At salinities of 9 and 19, *C. closterium* became stiffer and hydrophobic, whereas at salinities of 27 and 38, it behaved softer and hydrophilic, which might be related to a molecular change in the released biopolymers. This comprehensive study

provided a fundamental biophysical understanding of the adaptive mechanisms of individual algal species to changing salinity. Such understanding offers the basis for deciphering the complex interactions between abiotic stressors on microalgae in marine systems. The abovementioned changes in microalgal response showed that cell surface properties and behavior could be considered as markers of stress in marine communities and could be used to predict the effects of climate change on aquatic communities.

Supplementary Information The online version contains supplementary material available at https://doi.org/10.1007/s10811-022-02734-x.

Acknowledgements This work is supported by the Croatian Science Foundation Project "From algal cell surface properties to stress markers for aquatic ecosystems" (IP-2018-01-5840). The authors acknowledge networking in the COST action CA18238.

Data availability The datasets generated during the current study are available from the corresponding author.

References

Ahmed F, Zhou W, Schenk PM (2015) *Pavlova lutheri* is a high-level producer of phytosterols. Algal Res 10:210–217

Arata PX, Alberghina J, Confalonieri V, Errea MI, Estevez JM, Ciancia M (2017) Sulfated polysaccharides in the freshwater green macroalga *Cladophora surera* not linked to salinity adaptation. Front Plant Sci 8:1972–1982

Aratboni AH, Rafiei N, García-Granados R, Alemzadeh A, Morones-Ramirez J (2019) Biomass and lipid induction strategies in microalgae for biofuel production and other applications. Microb Cell Fact 18:178–195

Armbrust E (2009) The life of diatoms in the world's oceans. Nature 459:185–192

Atkinson D, Ciotti BJ, Montagnes DJS (2003) Protists decrease in size linearly with temperature: ca. 2.5% degrees C-1. Proc Roy Soc B 270:2605–2611

Aquino RS, Grativol C, Mourão PAS (2011) Rising from the sea: Correlations between sulfated polysaccharides and salinity in plants. PLoS One 6:e18862

Baek SH, Jung SW, Shin K (2011) Effects oftemperature and salinity on growth of *Thalassiosira pseudonana* (Bacillariophyceae) isolated from ballast water. J Freshwater Ecol 26:547–552

Bautista-Chamizo E, Sendra M, Cid Á, Seoane M, Romano de Orte M, Riba I (2018) Will temperature and salinity changes exacerbate the effects of seawater acidification on the marine microalga *Phaeodactylum tricornutum*? Sci Total Environ 634:87–94

Barati B, Gan S-Y, Lim P-E, Beardall J, Phang S-M (2019) Green algal molecular responses to temperature stress. Acta Physiol Plant 41:26–45

Benavente-Valdés JR, Aguilar C, Contreras-Esquivel JC, Méndez Zavala A, Montanez JC (2016) Strategies to enhance the production of photosynthetic pigments and lipids in chlorophycae species. Biotechnol Rep 10:117–125

Bligh EG, Dyer WJ (1959) A rapid method of total lipid extraction and purification. Can J Biochem Physiol 37:911–917

Borowitzka MA, Siva CJ (2007) The taxonomy of the genus *Dunaliella* (Chlorophyta, Dunaliellales) with emphasis on the marine and halophilic species. J Appl Phycol 19:567–590

Borowitzka MA (2018a) Biology of Microalgae. In: Levine IA, Fleurence J (eds) Microalgae in health and disease prevention. Academic Press, London, pp 23–72

Borowitzka MA (2018b) The "stress" concept in microalgal biology—homeostasis, acclimation and adaptation. J Appl Phycol 30:2815–2825

De Carvalho CCCR, Caramujo MJ (2018) The various roles of fatty acids. Molecules 23:2583–2619

Decho AW, Gutierrez T (2017) Microbial extracellular polymeric substances (EPSs) in ocean systems. Front Microbiol 8:922–950

El-Kassas HY, El-Sheekh MM (2016) Induction of the synthesis of bioactive compounds of the marine alga *Tetraselmis tetrathele* (West) Butcher grown under salinity stress. Egypt J Aquat Res 42:385–391

Falkowski P, Katz M, Knoll A, Quigg A, Raven J, Schofield O, Taylor F (2004) The evolution of modern eukaryotic phytoplankton. Science 305:354–360

Foflonker F, Mollegard D, Ong M, Su Yoon H, Bhattacharya D (2018) Genomic analysis of *Picochlorum* species reveals how microalgae may adapt to variable environments. Mol Biol Evol 35:2702–2711

Francavilla M, Trotta P, Luque R (2010) Phytosterols from *Dunaliella tertiolecta* and *Dunaliella salina*: a potentially novel industrial application. Bioresour Technol 101:4144–4150

Fu W, Paglia G, Magnúsdóttir M, Steinarsdóttir EA, Gudmundsson S, Palsson BØ, Brynjólfsson S (2014) Effects of abiotic stressors on lutein production in the green microalga *Dunaliella salina*. Microb Cell Fact 13:3

Gašparović B, Kazazić SP, Cvitešić A, Penezić A, Frka S (2015) Improved separation and analysis of glycolipids by Iatroscan thin-layer chromatography–flame ionization detection. J Chromatogr A 1409:259–267

Gašparović B, Kazazić SP, Cvitešić A, Penezić A, Frka S (2017) Corrigendum to "Improved separation and analysis of glycolipids by Iatroscan thin-layer chromatography–flame ionization detection" [J Chromatogr A 1409 (2015) 259–267]. J Chromatogr A 1521:168–169

Glaser K, Karsten U (2020) Salinity tolerance in biogeographically different strains of the marine benthic diatom *Cylindrotheca closterium* (Bacillariophyceae). J Appl Phycol 32:3809–3816

Griffiths MJ, Harrison STL (2009) Lipid productivity as a key characteristic for choosing algal species for biodiesel production. J Appl Phycol 21:493–507

Guillard RRL (1975) Culture of phytoplankton for feeding marine invertebrates. In: Smith WL, Chanley MH (eds) Culture of Marine Invertebrate Animals. Plenum Press, NY, pp 29–60

Guschina IA, Harwood JL (2006) Lipids and lipid metabolism in eukaryotic algae. Prog Lipid Res 45:160–186

Gustavs L, Eggert A, Michalik D, Karsten U (2010) Physiological and biochemical responses of green microalgae from different habitats to osmotic and matric stress. Protoplasma 243:3–14

Guzman-Murillo M, Ascencio F (2001) Enzyme-linked, biotin-streptavidin bacterial-adhesion assay for Helicobacter pylori lectin-like interactions with cultured cells. J Microbiol Biotechnol 11:35–39

Helm MM, Bourne N, Lovatelli A, Fisheries and Aquaculture Management Division, (2004) The hatchery culture of bivalves: a practical manual. FAO, Rome

Hunter KA, Liss PS (1981) Polarographic measurement of surface-active material in natural waters. Water Res 15:203–215

Hyung J-H, Kim E-J, Moon S-J, Kang NS, Park J (2021) *Tetraselmis jejuensis* sp. nov. (Chlorodendrophyceae), a euryhaline microalga found in supralittoral tide pools at Jeju Island, Korea. Plants 10:1289

Israelachvili JN (1992) Intermolecular forces & surface forces. Academic Press, New York

Ivošević N, Tomaić J, Žutić V (1994) Organic droplets at an electrified interface: critical potentials of wetting measured by polarography. Langmuir 7:2415–2418

Ivošević DeNardis N, Žutić V, Svetličić V, Frkanec R, Tomašić J (2007) In situ amperometric characterization of liposome suspensions with concomitant oxygen reduction. Electroanalysis 19:2444–2450

Ivošević DeNardis N, Ružić I, Pečar- Ilić J, El Shawish S, Ziherl P (2012) Reaction kinetics and mechanical models of liposome adhesion at charged interface. Bioelectrochemistry 88:48–56

Ivošević DeNardis N, Pečar Ilić J, Ružić I, Pletikapić G (2015) Cell adhesion and spreading at a charged interface: Insight into the mechanism using surface techniques and mathematical modelling. Electrochim Acta 176:743–754

Ivošević DeNardis N, Pečar Ilić J, Ružić I, Novosel N, Mišić Radić T, Weber A, Kasum D, Pavlinska P, Katalin Balogh R, Hajdu B, Marček Chorvátová A, Gyurcsik B (2019) Algal cell response to laboratory-induced cadmium stress: a multimethod approach. Eur Biophys J 48:231–248

Kefford B, Papas P, Crowther M, Nugegoda D (2002) Are salts toxicants? Australas J Ecotoxicol 8:63–68

Kim S-K (ed) (2015) Handbook of marine microalgae. Academic Press, London

Kirst GO (1990) Salinity tolerance of eukaryotic marine algae. Annu Rev Plant Physiol 41:21–53

Kovač S, Kraus R, Geček S, Žutić V (2000) Cell suspension as a model system for electrochemical analysis. Croat Chem Acta 73:279–291

Litchman E, Klausmeier CA, Yoshiyama K (2009) Contrasting size evolution in marine and freshwater diatoms. Proc Nat Acad Sci 106:2665–2670

Ma Z, Helbling EW, Li W, Villafañe VE, Gao K (2012) Motility and photosynthetic responses of the green microalga *Tetraselmis subcordiformis* to visible and UV light levels. J Appl Phycol 24:1613–1621

Mayali X, Franks PJS, Tanaka Y, Azam F (2008) Bacteria-induced motility reduction in *Lingulodinium polyedrum* (Dinophyceae). J Phycol 44:923–92836

Medlin L, Kaczmarska I (2004) Evolution of the diatoms: V. Morphological and cytological support for the major clades and a taxonomic revision. Phycologia 43:245–270

Minhas AK, Hodgson P, Barrow CJ, Adholeya A (2016) A review on the assessment of stress conditions for simultaneous production of microalgal lipids and carotenoids. Front Microbiol 7:1–19

Mišić Radić T, Čačković A, Penezić A, Dautović J, Lončar J, Omanović D, Juraić K, Ljubešić Z (2021) Physiological and morphological response of marine diatom *Cylindrotheca closterium* (Bacillariophyceae) exposed to cadmium. Eur J Phycol 56:24–36

Novak T, Godrijan J, Marić Pfannkuchen D, Djakovac T, Medić N, Ivančić I, Mlakar M, Gašparović B (2019) Global warming and oligotrophication lead to increased lipid production in marine phytoplankton. Sci Total Environ 668:171–183

Novosel N, Kasum D, Žutinić P, Legović T, Ivošević DeNardis N (2020) Short-term effect of cadmium on the motility of three flagellated algal species. J Appl Phycol 32:4057–4067

Novosel N, Mišić Radić T, Zemla J, Lekka M, Čačković A, Kasum D, Legović T, Žutinić P, Gligora Udovič M, Ivošević DeNardis N (2021) Temperature-induced response in algal cell surface properties and behaviour: an experimental approach. J Appl Phycol 33:1–17

Novosel N, Ivošević DeNardis N (2021) Structural features of the algal cell determine adhesion behavior at a charged interface. Electroanalysis 6:1436–1443

Oliveira L, Bisalputra T, Antia NJ (1980) Ultrastructural observation of the surface coat of *Dunaliella tertiolecta* from staining with cationic dyes and enzyme treatments. New Phytol 85:385–392

Ozkan A, Berberoglu H (2013) Physico-chemical surface properties of microalgae. Colloids Surf B 112:287–293

Parra-Riofrío G, García-Márquez J, Casas-Arrojo V, Uribe-Tapia E, Abdala-Díaz RT (2020) Antioxidant and cytotoxic effects on tumor cells of exopolysaccharides from *Tetraselmis suecica* (Kylin) Butcher grown under autotrophic and heterotrophic conditions. Mar Drugs 18:1–23

Pavlinska Z, Chorvat D, Mateasik A, Jerigova M, Velic D, Ivošević DeNardis N, Marcek Chorvatova A (2020) Fluorescence responsiveness of unicellular marine algae *Dunaliella* to stressors under laboratory conditions. J Biotechnol 324S:100018

Pillet F, Dague E, Pečar Ilić J, Ružić I, Rols M-P, Ivošević DeNardis N (2019) Changes in nanomechanical properties and adhesion dynamics of algal cells during their growth. Bioelectrochemistry 128:154–162

Pletikapić G, Berquand A, Mišić Radić T, Svetličić V (2012) Quantitative nanomechanical mapping of marine diatom in seawater using peak force tapping atomic force microscopy. J Phycol 48:174–185

Pletikapić G, Ivošević DeNardis N (2017) Application of surface analytical methods for hazardous situation in the Adriatic Sea: Monitoring of organic matter dynamics and oil pollution. Nat Hazards Earth Syst Sci 17:31–44

R Core Team (2020) R: A language and environment for statistical computing. R Foundation for Statistical Computing, Vienna, Austria.https://www.R-project.org/

Rogowska A, Szakiel A (2020) The role of sterols in plant response to abiotic stress. Phytochem Rev 19:1525–1538

Sader JE, Larson I, Mulvaney P, White LR (1995) Method for the calibration of atomic force microscope cantilevers. Rev Sci Instrum 66:3789–3798

Shetty P, Gitau MM, Maróti G (2019) Salinity stress responses and adaptation mechanisms in eukaryotic green microalgae. Cells 8:1657–1673

Sneddon IN (1965) The relation between load and penetration in the axisymmetric Boussinesq problem for a punch of arbitrary profile. Int J Eng Sci 3:47–57

Svetličić V, Ivošević N, Kovač S, Žutić V (2000) Charge displacement by adhesion and spreading of a cell: amperometric signals of living cells. Langmuir 16:8217–8220

Svetličić V, Balnois E, Žutić V, Chevalet J, Hozić Zimmermann A, Kovač S, Vdović N (2006) Electrochemical detection of gel microparticles in seawater. Croat Chem Acta 79:107–113

Thompson GA Jr (1996) Lipids and membrane function in green algae. Biochim Biophys Acta 1:17–45

Triadó-Margarit X, Casamayor E (2012) Genetic diversity of planktonic eukaryotes in high mountain lakes (Central Pyrenees, Spain). Environ Microbiol 14:2445–2456

Vanormelingen P, Vanelslander B, Sato S, Gillard J, Trobajo R, Sabbe K, Vyverman W (2013) Heterothallic sexual reproduction in the model diatom *Cylindrotheca*. Eur J Phycol 48:93–105

Venckus P, Cicchi B, Chini Zittelli G (2021) Effects of medium salinity on growth and biochemical composition of the green microalga *Tetraselmis suecica*. J Appl Phycol 33:1–9

Wei S, Bian Y, Zhao Q, Chen S, Mao J, Song C, Cheng K, Xiao Z, Zhang C, Ma W, Zou H, Ye M, Dai S (2017) Salinity-induced palmella formation mechanism in halotolerant algae *Dunaliella salina* revealed by quantitative proteomics and phosphoproteomics. Front Plant Sci 8:810

Xiao R, Zheng Y (2016) Overview of microalgal extracellular polymeric substances (EPS) and their applications. Biotechnol Adv 34:1225–1244

Zelazny AM, Shaish A, Pick U (1995) Plasma membrane sterols are essential for sensing osmotic changes in the halotolerant alga *Dunaliella*. Plant Physiol 109:1395–1403

Žutić V, Kovač S, Svetličić V (1993) Heterocoalescence between organic microdroplets and charged conductive interface. J Electroanal Chem 349:173–186

Žutić V, Ivošević N, Svetličić V, Long RA, Azam F (1999) Film formation by marine bacteria at a model fluid interface. Aquat Microb Ecol 17:231–238

Žutić V, Svetličić V, Ivošević N, Hozić A, Pečar O (2004) Northern Adriatic mesocosm experiment Rovinj 2003: dynamics of organic microparticles studied by the electrochemical technique. Period Biol 106:67–74